# Proton drip-line calculations and the *rp* process

B. A. Brown, R. R. C. Clement, H. Schatz, and A. Volya
*Department of Physics and Astronomy and National Superconducting Cyclotron Laboratory, Michigan State University, East Lansing, Michigan 48824-1321*

W. A. Richter
*Department of Physics, University of Stellenbosch, Stellenbosch 7600, South Africa*

(Received 23 July 2001; revised manuscript received 19 December 2001; published 19 March 2002)

One-proton and two-proton separation energies are calculated for proton-rich nuclei in the region $A=41-75$. The method is based on Skyrme Hartree-Fock calculations of Coulomb displacement energies of mirror nuclei in combination with the experimental masses of the neutron-rich nuclei. The implications for the proton drip line and the astrophysical *rp* process are discussed. This is done within the framework of a detailed analysis of the sensitivity of *rp* process calculations in type I x-ray burst models on nuclear masses. We find that the remaining mass uncertainties, in particular for some nuclei with $N=Z$, still lead to large uncertainties in calculations of x-ray burst light curves. Further experimental or theoretical improvements of nuclear mass data are necessary before observed x-ray burst light curves can be used to obtain quantitative constraints on ignition conditions and neutron star properties. We identify a list of nuclei for which improved mass data would be most important.

DOI: 10.1103/PhysRevC.65.045802 PACS number(s): 21.10.Dr, 26.50.+x, 97.60.Jd

## I. INTRODUCTION

The masses for the proton-rich nuclei above $A=60$ have not yet been measured. However, they are important for the astrophysical rapid-proton capture (*rp*) process [1] that follows a path in nuclei near $N=Z$ for $A=60-100$. The *rp* process is the dominant source of energy in type I x-ray bursts, and it determines the crust composition of accreting neutron stars [2–6]. It may also be responsible for the *p* process nucleosynthesis of a few proton-rich stable nuclei in the $A=74-98$ mass range. In the absence of experimental masses for the proton-rich nuclei, one often uses the masses based upon the Audi-Wapstra extrapolation (AWE) method [7]. In this paper, we use the displacement-energy method [8–11] to obtain the proton-rich masses with the Skyrme Hartree-Fock model for the displacement energies. The displacement energy is the difference in the binding energies (BE) of mirror nuclei for a given mass *A* and isospin *T*,

$$D(A,T)=BE(A,T_z^<)-BE(A,T_z^>), \tag{1}$$

where $T=|T_z^<|=|T_z^>|$, $BE(A,T_z^<)$ is the binding energy of the proton-rich nucleus and $BE(A,T_z^>)$ is the binding energy of the neutron-rich nucleus. The displacement energy can be much more accurately calculated than the individual BE in a variety of models since it depends mainly on the Coulomb interaction. In particular, we will use the spherical Hartree-Fock model based upon the recent Sk*X* set of Skyrme parameters [12], with the addition of charge-symmetry breaking (CSB), Sk$X_{csb}$ [13]. With the addition of CSB these calculations are able to reproduce the measured displacement energies for all but the lightest nuclei to within an rms deviation of about 100 keV [13]. In the $A=41-75$ mass region the mass (binding energy) of most of the neutron-rich nuclei are experimentally usually known to within 100 keV or better (the only exception being $^{71}$Br for which we use the AWE). Thus we combine the experimental binding energy for the neutron-rich nucleus $BE(A,T_z^>)_{exp}$ together with the Hartree-Fock value for $D(A,T)_{HF}$ to provide an extrapolation for the proton-rich binding energy

$$BE(A,T_z^<)=D(A,T)_{HF}+BE(A,T_z^>)_{\rm exp}. \tag{2}$$

The method is similar to the one used by Ormand [10] for the proton-rich nuclei with $A=46-70$. In Ref. [10] the displacement energies are based upon shell-model configuration mixing that includes Coulomb and CSB interactions with parameters for the single-particle energies and strengths that are fitted to this mass region. In the present paper, which covers the region $A=41-75$, the displacement energies are based upon Skyrme Hartree-Fock calculations with a global set of parameters that are determined from the properties of closed-shell nuclei and nuclear matter. The CSB part of the interaction has one parameter that was adjusted to reproduce the displacement energies in the $A=48$ mass region [13].

The displacement energies for all but the lightest nuclei can be reproduced with the constant CSB interaction given in Ref. [13], and we use the same CSB interaction for the extrapolations to higher mass discussed here.

The calculations presented here are relevant for the masses of proton-rich nuclei via their connection with their mirror neutron-rich analogues. We are not able to improve upon the masses of nuclei with $N=Z$, and as will be discussed, the relative large errors that remain for the $^{64}$Ge and $^{68}$Se masses provide now the dominant uncertainty in the *rp* process calculations.

Details of the Hartree-Fock (HF) calculations will be discussed, and a comparison between the calculated and experimental displacement energies for the $A=41-75$ mass region will be made. Then the extrapolations for the proton-rich masses and the associated one- and two-proton separation energies will be presented. The proton drip line that is estab-

 ©2002 The American Physical Society

lished by this extrapolation will be compared to experiment, and the nuclei that will be candidates for one- and two-proton decay will be discussed. Finally, we explore the significance of the new extrapolation for the $rp$ process in type I x-ray bursts.

## II. DISPLACEMENT-ENERGY CALCULATIONS

The Sk$X_{csb}$ interaction is used to carry out Hartree-Fock calculations for all nuclei in the range $Z=20-38$ and $N=20-38$. The binding energies are then combined in pairs to obtain theoretical displacement energies for $A=41-75$ and $T=1/2$ to $T=4$:

$$D(A,T)_{HF}=BE(A,T_z^<)_{HF}-BE(A,T_z^>)_{HF}. \qquad (3)$$

The calculation is similar to those presented in Ref. [13], but several refinements are made. The single-particle states in proton-rich nuclei become unbound beyond the proton drip line. In the nuclei we consider they are unbound by up to about 2 MeV. Since 2 MeV is small compared to the height of the Coulomb barrier (about 6 MeV at a radius of 7 fm), the states are ''quasibound'' and have a small proton-decay width (on the order of keV or smaller). To obtain the quasibound wave functions we put the HF potential in a box with a radius of 20 fm and a depth of 20 MeV. In all cases we consider, the dependence of the results on the form of the external potential is negligible as long as the radius is greater than about 10 fm and the potential depth is greater than about 10 MeV.

In Ref. [13] the occupation numbers of the spherical valence states were filled sequentially, and in this mass region they always occur in the order $f_{7/2}$, $p_{3/2}$, $f_{5/2}$, $p_{1/2}$, and $g_{9/2}$. We have improved on this scheme by carrying out an exact pairing (EP) calculation [14] at each stage of the HF iteration. The exact pairing model has recently been discussed in Ref. [14]. The EP method uses the single-particle energies from the HF calculation together with a fixed set of $J=0$, $T=1$ two-body matrix elements and gives the orbit occupations and the pairing correlation energy. The orbit occupations are then used together with the HF radial wave functions to calculate the nucleon densities that go into the Skyrme energy density functional. This procedure is iterated until convergence (about 60 iterations). The pairing is calculated for protons and neutrons with the same set of two-body matrix elements taken from the FPD6 interaction for the $pf$ shell [15] and the Bonn-$C$ renormalized $G$ matrix for the matrix elements involving the $g_{9/2}$ orbit [16]. For those nuclei we consider here, the occupation of the $g_{9/2}$ orbit is always small. It is known that deformed components of the $2s$-$1d$-$0g$ shell are essential for the nuclear ground states above $A=76$ as indicated by the sudden drop in the energy of the $2^+$ state from 709 keV in $^{72}$Kr to 261 keV in $^{76}$Sr [17]. Thus, we do not go higher than $A=76$. In addition, one cannot always use Eq. (2) above $A=76$ since many of the masses of the neutron-rich nuclei are not known experimentally.

The results we obtain are not very sensitive to the strength of the pairing interaction and the associated distribution of the nucleons between the $p$ and $f$ orbits, since these orbits have similar rms radii and single-particle Coulomb shifts. For example, a 20% change in the strength of the pairing interaction results in displacement-energy changes of less than 20 keV. If pairing is removed, the displacement energies can change by up to about 100-keV. Thus, at the level of 100 keV accuracy pairing should be included, but it is not a crucial part of the model.

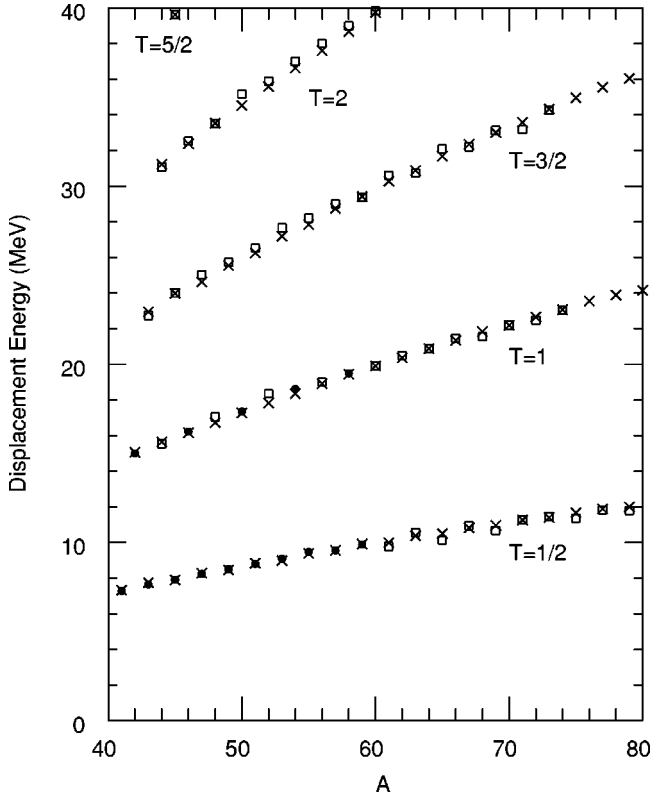


FIG. 1. Calculated displacement energies (crosses) as a function of mass number. They are compared to experimental data (filled circles) and to values based upon the Audi-Wapstra extrapolations (squares).

A final refinement has been to add a Coulomb pairing contribution to the proton-proton $J=0$ matrix elements. The two-body Coulomb matrix elements were calculated in a harmonic-oscillator basis. The Coulomb pairing is then defined as the difference of the diagonal $J=0$ matrix elements from the $(2J+1)$ weighted average (which corresponds to the spherical part of the Coulomb potential that is in the HF part of the calculation). The Coulomb pairing matrix elements are 50–100 keV.

In Fig. 1 the calculated displacement energies (crosses) are shown in comparison with experiment (filled circles) in cases where both proton- and neutron-rich masses have been measured and with the AWE (squares) in cases where the mass of the proton-rich nucleus is based upon the AWE. The corresponding differences between experiment and theory are shown in Fig. 2 including the experimental or AWE error bars. It can be seen that when the displacement energy is measured the agreement with the calculation is excellent to within an rms deviation of about 100 keV. The most exceptional deviation is that for $A=54$ involving the $^{54}$Ni-$^{54}$Fe

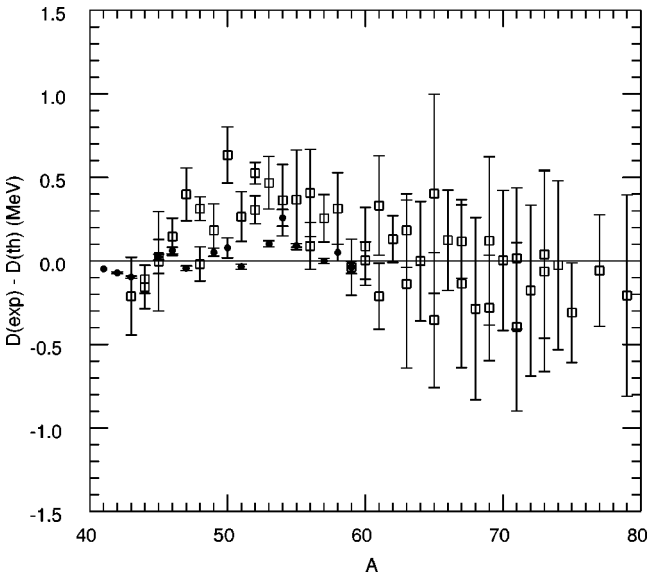


FIG. 2. Difference between the calculated displacement energies and experiment (filled circles) or values based on the the Audi-Wapstra extrapolations (squares).

mirror pair; a confirmation of the experimental mass for $^{54}$Ni (which has a 50 keV error) would be worthwhile. The comparison based upon the AWE (squares) shows a much larger deviation with typically up to 500-keV differences, but the AWE error assumed is sometimes (but not always) large enough to account for the spread. The implication of this comparison is that the error in the HF extrapolation of the displacement energies is probably much less than the error in the AWE of the displacement energies. In particular, one notices in Fig. 1 in the region $A=60-75$ that the displacement energy based upon the AWE shows a small oscillation that is not present in the HF calculation and which is not present in the experimental data for $A<60$.

## III. PROTON-RICH MASSES AND SEPARATION ENERGIES

The next step is to use Eq. (2) to calculate the binding energy of the proton-rich nuclei based upon the HF calculation of the displacement energy together with the experimental binding energy of the neutron-rich nucleus [7,18]. The only neutron-rich nucleus whose mass is not yet experimentally measured is $^{71}$Br for which we use the AWE value. The binding energies for the HF extrapolations for the proton-rich nuclei are given an error based upon the experimental error of the neutron-rich binding energy folded in quadrature with an assumed theoretical error of 100 keV.

The HF extrapolated set of binding energies for proton-rich nuclei together with the experimental binding energies for nuclei with $N=Z$ and neutron-rich nuclei provides a complete set of values from which the one- and two-proton separation energies are obtained. The masses for the $N=Z$ nuclei $^{66}$As, $^{68}$Se, $^{70}$Br, are not measured and we use the AWE value. The mass for $^{74}$Rb has a relatively large experimental error.

Results for the one- and two-proton separation energies are shown in Fig. 3. The first line in each box is the one-proton separation energy (and the associated error) based upon the AWE with the associated error. The second line is the one-proton separation energy based upon the HF extrapolation, and the third line is the two-proton separation energy based upon the HF extrapolation. The error in the separation energies is the error for the binding energies of the parent and daughter nuclei folded in quadrature.

The double line in Fig. 3 is the proton drip line beyond which the one-proton separation energy and/or the two-proton separation energy becomes negative. However, due to the Coulomb barrier, some of the nuclei beyond the proton drip line may have lifetimes that are long enough to be able to observe them in radioactive beam experiments. The observation of $^{65}$As in the experiment of Blank *et al.* [19] excludes half-lifes that are much shorter than 1 $\mu$s that indicates that it is unbound by less than 400 keV. The identification of $^{65}$As as a $\beta$ emitter by Winger *et al.* [20] together with the nonobservation of emitted protons by Robertson *et al.* [21] indicates that it is unbound by less than 250 keV. Both limits are compatible (within error) with the HF results given in Fig. 3. The nonobservation of $^{69}$Br in the radioactive beam experiments of Blank *et al.* [19] and Pfaff *et al.* [22] means that its lifetime is less than 24 ns, which implies that it is proton unbound by more than 500 keV [22]. This is compatible with the HF result shown in Fig. 3. The nonobservation of $^{73}$Rb in the experiments of Mohar *et al.* [23], Jokinen *et al.* [24], and Janas *et al.* [25] gives an upper limit of 30 ns for the half-life, which implies that $^{73}$Rb is proton unbound by more than 570 keV, again in agreement (within error) of the present HF result. Thus all of the current experimental data are consistent with our calculations.

The proton drip line has not yet been reached for most $Z$ values. Beyond the proton drip line there are several candidates for nuclei that should be explored for one-proton emission: $^{54}$Cu, $^{58}$Ge, $^{64}$As, $^{68}$Br, $^{69}$Br, $^{72}$Rb, and $^{73}$Rb. The most promising candidates for the illusive diproton emission (in addition to $^{48}$Ni [8,10]) are $^{64}$Zn, $^{59}$Ge, $^{63}$Se, $^{67}$Kr, and $^{71}$Sr. Estimated lifetime ranges for these diproton decays are given by Ormand [10].

## IV. IMPLICATIONS FOR THE *rp* PROCESS

The $rp$ process beyond Ni plays a critical role during hydrogen burning at high temperatures and densities on the surface of accreting neutron stars in x-ray bursters and x-ray pulsars [2–6]. Nuclear masses are among the most important input parameters in $rp$ process calculations, as they sensitively determine the balance between proton capture and the inverse process, $(\gamma,p)$ photodisintegration. It is this $(\gamma,p)$ photodisintegration that prevents the $rp$ process from continuing via proton captures, once a nucleus close to the proton drip line is reached. This nucleus then becomes a ''waiting point'' as the $rp$ process has to proceed at least in part, via the slow $\beta^+$ decay. The effective lifetime of the waiting points in the $rp$ process determines the overall processing time scale, energy generation, and the final abundance distribution. At a waiting point nucleus $(Z,N)$, a local $(p,\gamma)$-$(\gamma,p)$ equilibrium is established with the following

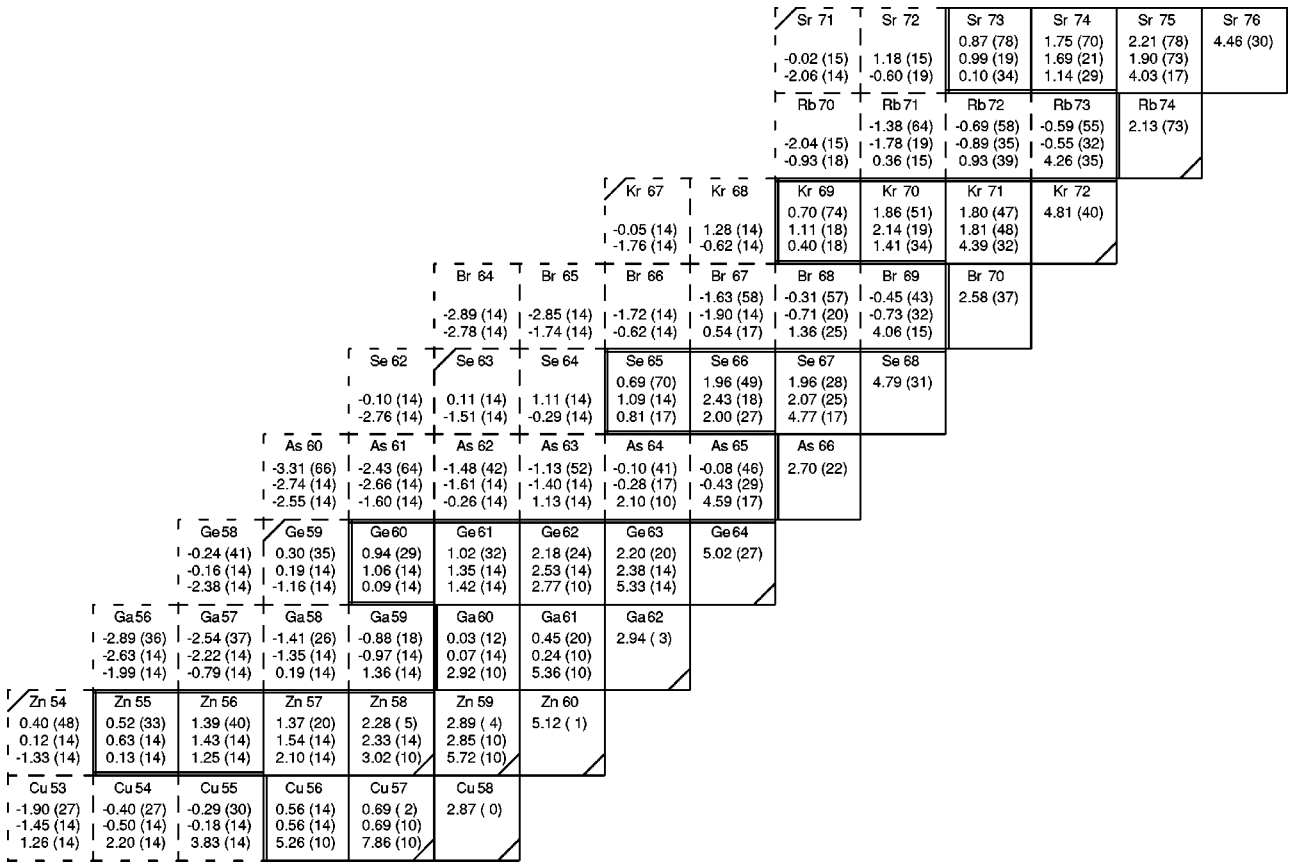


FIG. 3. A section of the mass chart for $N=Z$ and proton-rich nuclei showing: (line 1): the one-proton separation energy (followed by the associated error) based upon AWE; (line 2): the one-proton separation energy based upon the present HF calculations; and (line 3): the two-proton separation energy based upon the HF calculations. The line in the lower right-hand corner indicates that the mass has been measured for this nucleus. A line in the upper left-hand corner indicates that this nucleus is a candidate for diproton decay.

isotones $(Z+1,N)$, $(Z+2,N)$. The effective proton capture flow destroying waiting point nuclei and reducing their lifetime is then governed by the Saha equation and the rate of the reaction leading out of the equilibrium. Because of the odd-even structure of the proton drip line two cases have to be distinguished [3]. For temperatures below $\approx 1.4$ GK equilibrium is only established with the following isotone $(Z+1,N)$. In this case, the destruction rate of the waiting point nucleus via proton captures $\lambda_{(Z,N)(p,\gamma)}$ is determined by the Saha equation and the proton-capture rate on the following isotone $(Z+1,N)$. The total destruction rate of the waiting point nucleus $(Z,N)$ is then given by the sum of proton-capture and $\beta$-decay rates,

$$\lambda=\lambda_\beta+Y_p^2\rho^2N_A^2\left(\frac{2\pi\hbar^2}{\mu_{(Z,N)}kT}\right)^{3/2}\frac{G_{(Z+1,N)}(T)}{(2J_p+1)G_{(Z,N)}(T)}\times\exp\left(\frac{Q_{(Z,N)(p,\gamma)}}{kT}\right)\langle\sigma v\rangle_{(Z+1,N)(p,\gamma)}, \tag{4}$$

$\lambda_\beta$ is the $\beta$-decay rate of nucleus $(Z,N)$, $Y_p$ the hydrogen abundance, $\rho$ the mass density, $J_p$ the proton spin, $G_{(Z,N)}$ the partition function of nucleus $(Z,N)$, $T$ the temperature, $\mu_{(Z,N)}$ the reduced mass of nucleus $(Z,N)$ plus proton, $Q_{(Z,N)(p,\gamma)}$ the proton capture $Q$ value of the waiting point nucleus, and $\langle\sigma v\rangle_{(Z+1,N)(p,\gamma)}$ the proton-capture rate on the nucleus $(Z+1,N)$. For higher temperatures local equilibrium is maintained between the waiting point nucleus $(Z,N)$ and the next two following isotones $(Z+1,N)$ and $(Z+2,N)$. In this case, $\lambda_{(Z,N)(p,\gamma)}$ is given by the Saha equation and the $\beta$-decay rate of the final nucleus $\lambda_{(Z+2,N)\beta}$, and the total destruction rate $\lambda$ of the waiting point nucleus becomes

$$\lambda=\lambda_\beta+Y_p^2\rho^2N_A^2\left(\frac{2\pi\hbar^2}{kT}\right)^3\mu_{(Z,N)}^{-3/2}\mu_{(Z+1,N)}^{-3/2}\times\frac{G_{(Z+2,N)}(T)}{(2J_p+1)^2G_{(Z,N)}(T)}\exp\left(\frac{Q_{(Z,N)(2p,\gamma)}}{kT}\right)\lambda_{(Z+2,N)\beta}. \tag{5}$$

In both cases, the destruction rate of a waiting point nucleus depends exponentially either on its one-proton-capture $Q$ value $Q_{(Z,N)(p,\gamma)}$ or two-proton-capture $Q$ value $Q_{(Z,N)(2p,\gamma)}$. Nuclear masses therefore play a critical role in determining the $rp$ process waiting points and their effective lifetimes.

It has been shown before that the most critical waiting point nuclei for the $rp$ process beyond Ni are $^{64}$Ge, $^{68}$Se, and $^{72}$Kr [3]. With the exception of $^{56}$Ni and $^{60}$Zn, these nuclei are by far the longest-lived isotopes in the $rp$ process

path. The reason for those three nuclei being the most critical ones is that with increasing charge number the $N=Z$ line moves closer to the proton drip line and away from stability. Therefore, proton-capture $Q$ values on even-even $N=Z$ nuclei, which are favored in the $rp$ process because of the odd-even structure of the proton drip line, decrease with increasing charge number, while the $\beta$-decay $Q$ values become larger. $^{64}$Ge, $^{68}$Se, and $^{72}$Kr happen to be located in the ''middle,'' where proton-capture $Q$ values are already low enough to suppress proton captures and allow $\beta$ decay to compete, but at the same time $\beta$-decay $Q$ values are still small enough for half-lifes to be long compared to $rp$ process time scales. The critical question is to what degree proton captures can reduce the long $\beta$-decay lifetimes of $^{64}$Ge (63.7 s half-life), $^{68}$Se (35.5 s half-life), and $^{72}$Kr (17.2 s half-life). As Eqs. (4) and (5) show, the answer depends mainly on the one- and two-proton-capture $Q$ values. Unfortunately, experimental data exist for none of the relevant $Q$ values. The only available experimental information are upper limits of the one-proton-capture $Q$ values of $^{68}$Se and $^{72}$Kr from the nonobservation of $^{69}$Br [19,22] and $^{73}$Rb [23–25], and the lower limits on the one-proton-capture $Q$ value on $^{65}$As from its identification as a $\beta$ emitter in radioactive beam experiments (see Sec. III). While these data provide some constraints, accurate $Q$ values are needed for the calculations and have to be predicted by theory. The new masses calculated in this paper cover exactly this critical mass range, and provide improved predictions for all the relevant $Q$ values in the $A=64$–$72$ mass region (see Fig. 3). As discussed in Sec. III, all of our new predictions are compatible with the existing experimental limits.

To explore the impact of the new mass predictions on $rp$ process models, we performed calculations with a one-dimensional, one-zone x-ray burst model [6,26]. Ignition conditions are based on a mass accretion rate of 0.1 times the Eddington accretion rate, an internal heat flux from the neutron star surface of 0.15 MeV/nucleon, an accreted matter metallicity of $10^{-3}$, and a neutron star with 1.4 solar masses and 10-km radius.

In principle, proton separation energies can influence the reaction flow in two ways. First, they affect the forward to reverse rate ratios for proton-capture reactions and the local $(p,\gamma)$-$(\gamma,p)$ equilibria through the $\exp(Q/kT)$ term in the Saha equation [in Eqs. (4) and (5)]. This leads to an exponential mass dependence of the waiting point lifetimes. Second, theoretical predictions of reaction rates $\langle \sigma v \rangle$ [in Eq. (4)] depend also on the adopted $Q$ values. In this paper we choose to take into account both effects. To explore the impact of $Q$ value uncertainties on proton-capture reaction rate calculations we use the statistical model code SMOKER [3]. Even though the nuclei in question are close to the proton drip line a statistical approach is justified in most cases because reaction rates tend to become important only for larger $Q$ values when a local $(p,\gamma)$-$(\gamma,p)$ equilibrium cannot be established. Then the level density tends to be sufficient for the statistical model approach. Based on the new reaction rates we then use our new $Q$ values to recalculate $(\gamma,p)$ photodisintegration rates via detailed balance as discussed in Ref. [3].

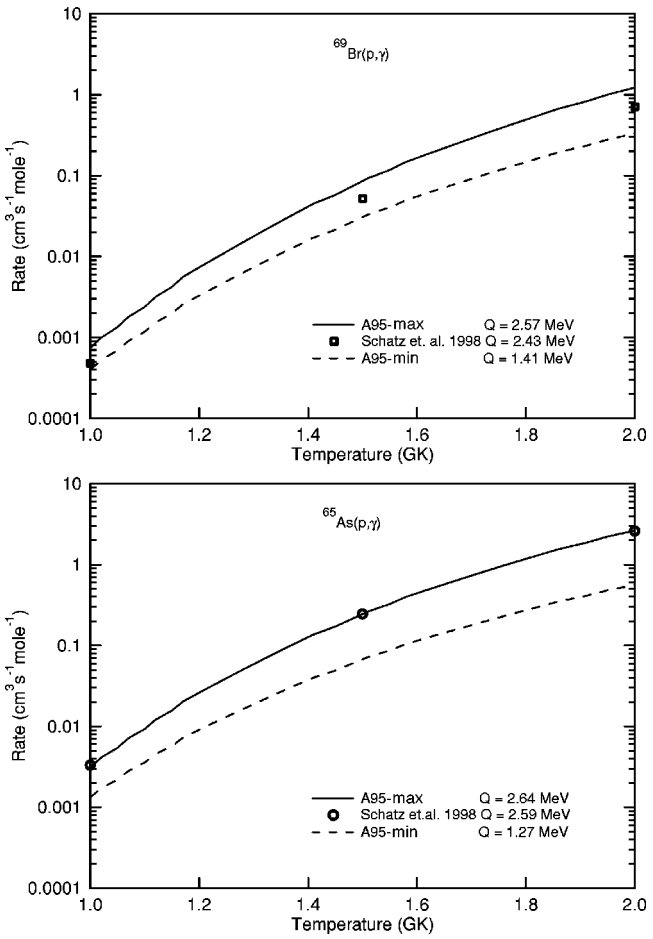


FIG. 4. Calculated $X(p,\gamma)$ rates for $X=^{65}$As and $X=^{69}$Br with associated $Q$ values shown in the legend. The astrophysical reaction rates were calculated with the statistical model code SMOKER.

For the relevant temperature range between 1–2 GK, our new proton-capture reaction rates vary in most cases not more than a factor of 2 within the explored mass uncertainties. An exception among the relevant reaction rates are the proton-capture rates on $^{65,66}$As, $^{69,70}$Br, and $^{73,74}$Rb. These rates show a somewhat stronger variation of typically a factor of 4–6 as the associated proton-capture $Q$ values are particularly uncertain. Figure 4 shows two examples for the $Q$-value dependence of statistical model reaction rates. Generally, a larger $Q$ value leads to larger rates. For reference, Fig. 4 also shows the rates listed in Ref. [3], which had been calculated using $Q$ values from the finite range droplet mass model (FRDM) 1992 [27].

To disentangle the different effects of mass uncertainties quantitatively we performed test calculations in which changes in masses were only taken into account in the calculation of the $(\gamma,p)$ photodisintegration rates, while the proton-capture rates were kept the same. These test calculations lead to very similar luminosity and burst time scale variations as presented in this paper. Discrepancies were at most 8% in the luminosity and 0.1% in the burst timescale. This can be understood from Eqs. (4) and (5). For example, a change of 1.37 MeV in the proton-capture $Q$ value changes the $^{65}$As reaction rate and therefore the lifetime of the $^{64}$Ge

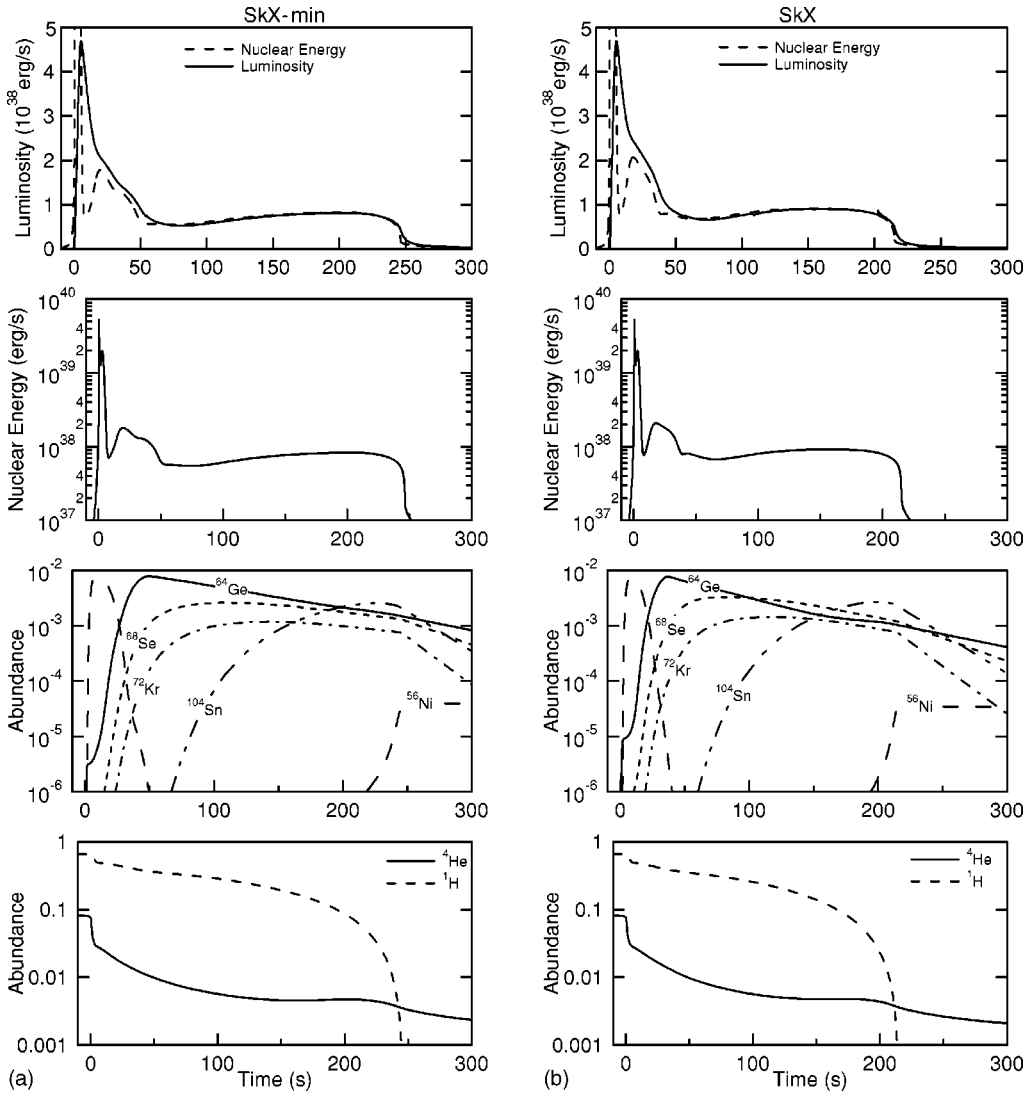


FIG. 5. Luminosity, nuclear energy generation rate, and the abundances of hydrogen, helium, and the critical waiting point nuclei as functions of time as predicted by our x-ray burst model for different sets of proton-capture $Q$ values. Shown are results for the sets Sk$X$-min, Sk$X$, and Sk$X$-max for the smallest, the recommended, and the largest proton-capture $Q$ values within the error bars of the mass predictions of this paper. A corresponding series is shown for the Audi & Wapstra 1995 mass evaluation (AW-min, AW, and AW-max). The $^{104}$Sn abundance indicates the operation of the SnSbTe cycle. Also, for comparison, the nuclear energy generation rate is shown as a dashed line together with luminosity, though it is off the scale shown during the peak of the burst. The mass of the accreted layer is $5.0\times10^{21}$ g.

waiting point nucleus by a factor of 3–4 [see Fig. 4 and Eq. (4)]. However, the same 1.37 MeV $Q$-value change in the $\exp(Q/kT)$ term in Eq. (5) would result in a lifetime change of six orders of magnitude (for a typical $kT=100$ keV). We therefore conclude that the impact of mass uncertainties on $rp$ process calculations through changes in theoretical reaction rate calculations within the statistical model is much smaller than the impact through changes in $(p,\gamma)/(\gamma,p)$ reaction rate ratios.

The following calculations were performed with different assumptions on masses beyond the $N=Z$ line from $Z=30$–38: Sk$X$ based on the mass predictions of this paper, Sk$X$-min with all proton-capture $Q$-values set to the lowest value, and Sk$X$-max with all proton-capture $Q$ values set to the highest values within the error bars of our binding energy predictions. A similar set of calculations has been performed for the mass extrapolations of Audi and Wapstra 1995 [7] (AW95) and are labeled AW, AW-min, and AW-max. Figure 5 shows the x-ray burst light curve, the nuclear energy generation rate, the abundances of the most important waiting point nuclei and the hydrogen and helium abundances as a function of time for all our calculations. As an example, Fig. 6 shows the time integrated reaction flow corresponding to the Sk$X$ calculation. While the $\alpha p$ and $rp$ processes below $^{56}$Ni are responsible for the rapid luminosity rise at the beginning of the burst, processing through the slow waiting points $^{64}$Ge, $^{68}$Se, $^{72}$Kr and the operation of the SnSbTe cycle (indicated by the $^{104}$Sn abundance) lead to an extended burst tail. The $rp$ process from $^{56}$Ni to $^{64}$Ge, and the slowdown at $^{64}$Ge lead to a pronounced peak in the energy generation rate around 25 s after burst maximum. In principle, the other waiting points have a similar effect, but the corre-

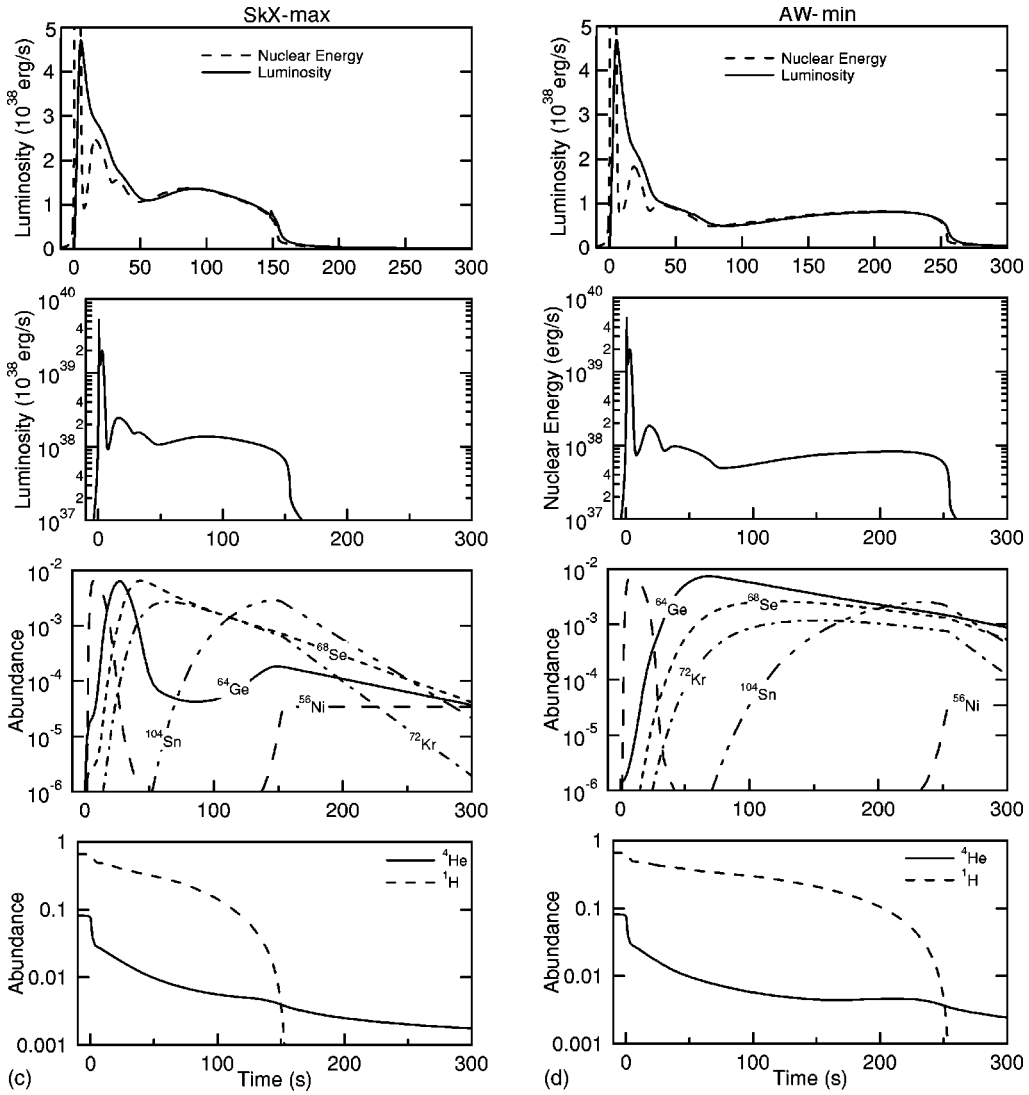


FIG. 5. (*Continued.*)

sponding peaks in the energy production are much wider and therefore not noticeable.

Figure 7 compares x-ray burst light curves for different assumptions on nuclear masses. Generally, lower proton-capture $Q$ values enhance photodisintegration and favor the waiting point nuclei in local equilibria. Both effects lead to a slower reaction flow and therefore to less luminous but longer lasting burst tails. Even though the uncertainties in our new mass predictions are significantly smaller than in AW95, they still allow for a burst length variation from 150–250 s and a luminosity variation of about a factor of 2 (Sk$X$-min and Sk$X$-max). The lower limit $Q$-value calculation with AW95 masses (AW-min) is similar to our lower limit (Sk$X$-min), but the larger uncertainties in the AW95 masses lead to large differences in the upper limits (Sk$X$-max and AW-max) and would imply significantly shorter bursts with much more luminous tails (AW-max). However, some of the large proton-capture $Q$ values in AW-max and to a lesser degree in Sk$X$-max are already constrained by the experiments on $^{69}$Br and $^{73}$Rb. If those constraints are taken into account one obtains the AW-max-expt and Sk$X$-max-expt calculations, respectively, which are also shown in Fig. 7. The Sk$X$-max-expt and AW-max-expt light curves are very similar.

The dependence of the light curves on the choice of proton-capture $Q$ values can be understood entirely from the changes in $\beta$ decay and proton-capture branchings of the main waiting points $^{64}$Ge, $^{68}$Se, and $^{72}$Kr shown in Table I. The calculations with the lower limits on proton-capture $Q$ values (Sk$X$-min and AW-min) do not differ much as they all predict that proton-captures do not play a role. However, for the upper limits sizable proton-capture branches occur and lead to significant reductions in the lifetimes of the waiting points. In our upper limit (Sk$X$-max) we obtain 26% proton capture on $^{68}$Se (via $2p$ capture) and 86% proton capture on $^{64}$Ge, while proton captures on $^{72}$Kr with 8%, play only a minor role. These branchings become even larger for the AW95 upper limit calculations (AW-max-expt and AW-max). Note that $\beta$ decay of $^{60}$Zn is negligible (see Table I) because proton capture dominates for the whole range of nuclear masses considered here.

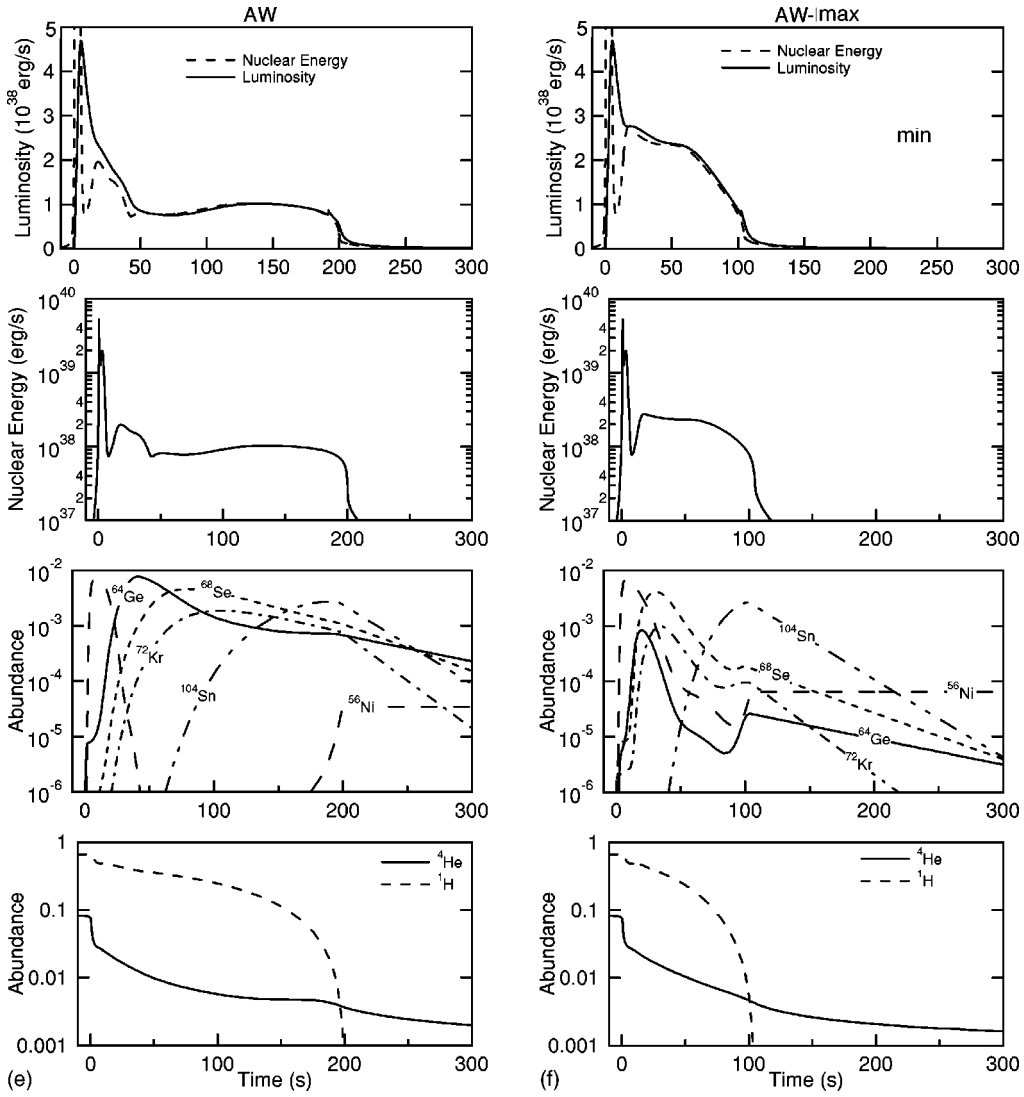


FIG. 5. (*Continued.*)

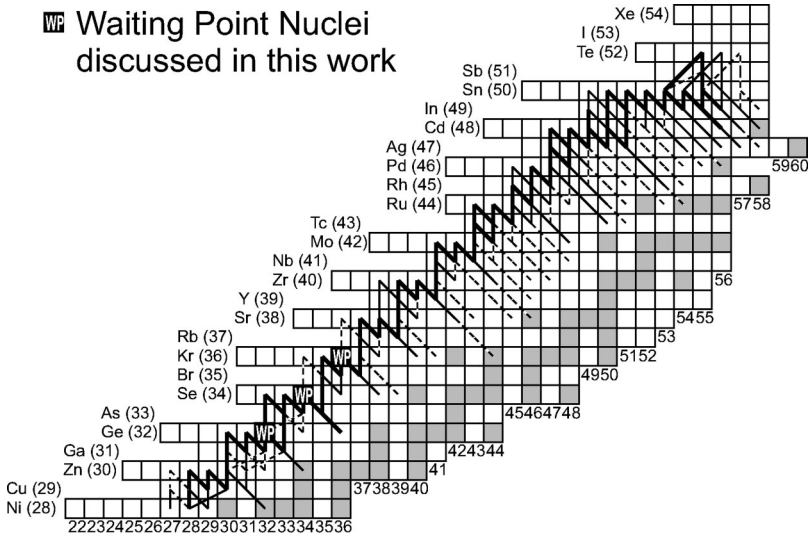


FIG. 6. Time integrated reaction flow beyond Ni during an x-ray burst calculated on the basis of our new mass predictions. Shown are flows of more than 10% (thick solid line), 1–10 % (thin solid line), and 0.1–10 % (dashed line) of the flow through the $3\alpha$ reaction. The key waiting points discussed in this paper are marked as well.

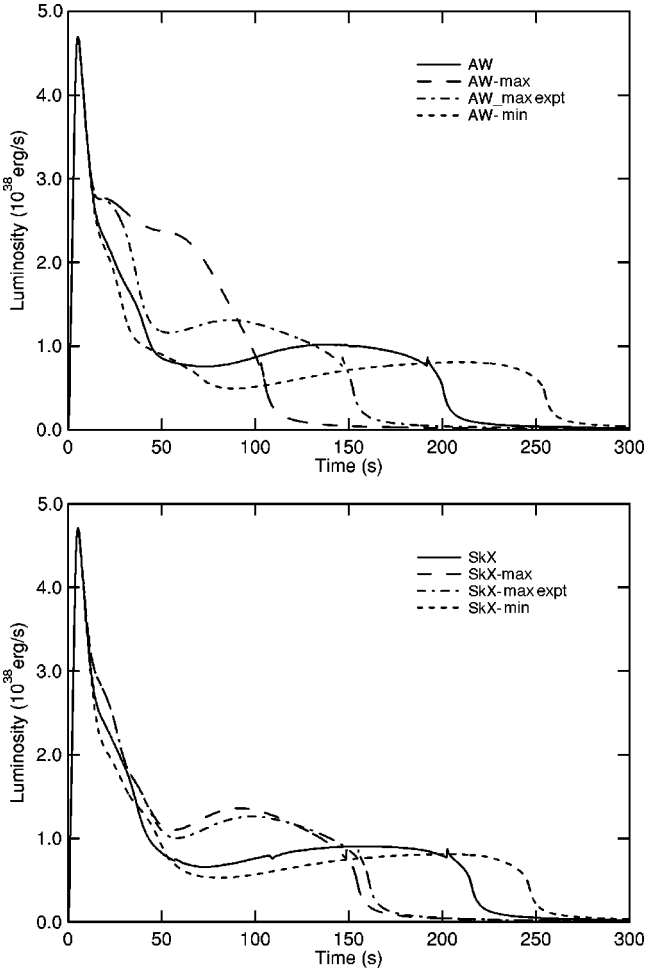


FIG. 7. X-ray burst luminosity as functions of time for model calculations with different assumptions on proton-capture $Q$ values in the Zn-Sr range: results on the upper panel are based on the Audi & Wapstra 1995 recommended masses (AW) and the largest (AW-max) and smallest (AW-min) proton-capture $Q$ values according to their error bars. AW-max-expt is identical to AW-max, but takes into account experimental limits on the proton-capture $Q$ values of $^{68}$Se and $^{72}$Kr. The lower panel shows the same set of calculations based on the mass predictions of this paper (Sk$X$ . . . ). The mass of the accreted layer is $5.0\times10^{21}$ g.

The importance of the one-proton-capture $Q$ values in the determination of lifetimes for $rp$ process waiting points has been discussed extensively before [3]. This importance is clearly expressed by the large changes in branching ratios and light curves when experimental constraints (which only exist for one-proton separation energies) are imposed on the AW-max calculations leading to AW-max-expt (Fig. 7 and Table I). However, the two-proton-capture $Q$ values can be equally important. For example, the proton-capture branching on $^{68}$Se changes by an order of magnitude from 2% in AW to 15% in AW-max-expt. This change is entirely due to the change in the $^{70}$Kr proton separation energy from 1.86 MeV in AW to 2.4 MeV in AW-max-expt as the proton-capture $Q$ value on $^{68}$Se is very similar (only 0.05 MeV difference). The reason for this sensitivity is the onset of photodisintegration of $^{70}$Kr that depends very sensitively on its proton separation energy. As soon as temperatures are sufficiently high for $^{70}\mathrm{Kr}(\gamma,2p)^{68}\mathrm{Se}$ to play a role, $^{68}$Se, $^{69}$Br, and $^{70}$Kr are driven into a local $(p,\gamma)$-$(\gamma,p)$ equilibrium. With rising temperature the proton capture on $^{68}$Se drops then quickly to zero, because the temperature independent and slow $\beta$ decay of $^{70}$Kr in Eq. (5) cannot provide a substantial leakage out of the equilibrium. This is different from the situation at lower temperatures described by Eq. (4) where a lower equilibrium abundance of $^{69}$Br at higher temperatures can be somewhat compensated by the increasing proton capture rate on $^{69}$Br. This effect is illustrated in Fig. 8 that shows the lifetime of $^{68}$Se against proton capture and $\beta$ decay as a function of temperature for different choices of proton-capture $Q$ values. The lifetime equals the $\beta$-decay lifetime for low temperatures because of slow proton-capture reactions, and at high temperatures because of the photodisintegration effect discussed above. For the AW masses, the low proton separation energy of $^{70}$Kr leads to strong photodisintegration already at temperatures around 1.15 GK before proton captures can play a role. Therefore, proton captures never reduce the lifetime significantly. For AW-max-expt, the only change is a larger $^{70}$Kr proton separation energy of 2.4 MeV. Though $^{69}$Br is unbound by 500 keV, proton captures can reduce the lifetime of $^{68}$Se by about a factor of 2 around 1.4 GK before photodisintegration sets in and starts inhibiting further proton captures. This can be compared with the upper limits of our predictions for proton separation energies (Sk$X$-max). The larger proton separation energy of $^{69}$Br allows an onset of proton captures at slightly lower temperatures, but the lower proton separation energy of $^{70}$Kr leads also to an onset of photodisintegration at somewhat lower temperatures thus effectively shifting the drop in lifetime by about 0.1 GK. Note that it is not only the amount of lifetime reduction, but also how well necessary conditions match the actual conditions during the cooling of the x-ray burst that determine the role of proton captures and therefore

TABLE I. Branchings for proton captures on the most important waiting point nuclei for different mass predictions from AW95 (AW) and this work Sk$X$. These branchings are the time integrated averages obtained from our x-ray burst model.

| Waiting point | Sk$X$ | Sk$X$-min–Sk$X$-max | AW-min–AW-max | AW-min–AW-max-expt |
|---|---|---|---|---|
| $^{60}$Zn | 95% | 91–97 % | 83–98 % | 83–99 % |
| $^{64}$Ge | 30% | 0.5–86 % | 0.0–98 % | 0.0–99 % |
| $^{68}$Se | 0.5% | 0.0–26 % | 0.0–74 % | 0.0–15 % |
| $^{72}$Kr | 0.0% | 0.0–8 % | 0.0–87 % | 0.0–8 % |

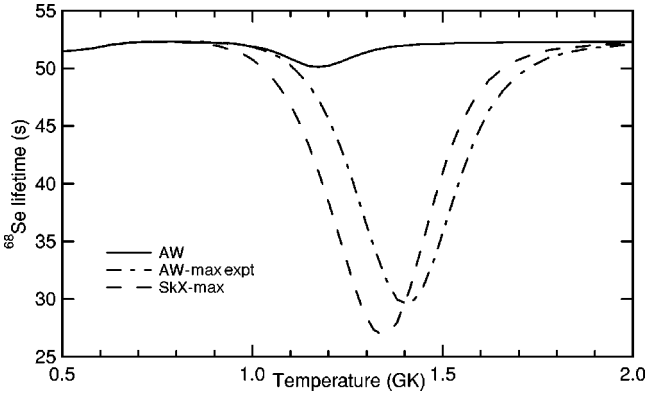


FIG. 8. Lifetime of $^{68}$Se against $\beta$ decay and proton capture for typical $rp$ process conditions during the burst tail (hydrogen abundance 0.35, density $6\times10^5$ g/cm$^3$) for three different assumptions on proton-capture $Q$ values on $^{68}$Se and $^{69}$Br: Audi & Wapstra 1995 recommended masses (AW), the largest proton-capture $Q$ values within the AW error bars but with experimental constraints on the $^{68}$Se$(p,\gamma)$ $Q$ value (AW-max-expt), and the largest proton-capture $Q$ values within the error bars of the predictions from this paper (Sk$X$-max).

the overall time scale of the $rp$ process. As Fig. 8 shows, both depends sensitively on the nuclear masses.

A long-standing question is how the nuclear physics and, in particular the properties of the long-lived waiting points $^{64}$Ge, $^{68}$Se, and $^{72}$Kr affect the end point of the $rp$ process. Even for our lowest-proton-capture $Q$ values where proton captures on $^{68}$Se and $^{72}$Kr become negligible, we still find that the $rp$ process reaches the SnSbTe cycle [6]. Figure 9 shows the final abundance distribution for the two extreme cases—our calculation with the slowest (Sk$X$-min) and the fastest (AW-max) reaction flow. In both cases, the most abundant mass number is $A=104$, which is due to accumulation of material in the SnSbTe cycle at $^{104}$Sn. The main difference between the abundance patterns are the abundances that directly relate to the waiting points at $A=64$, 68, and 72 and scale roughly with the waiting point lifetime. In addition, for AW-max nuclei in the $A=98$–103 mass range are about a factor of 3 more abundant because of the faster processing and the depletion of $A=64$, 68, and 72.

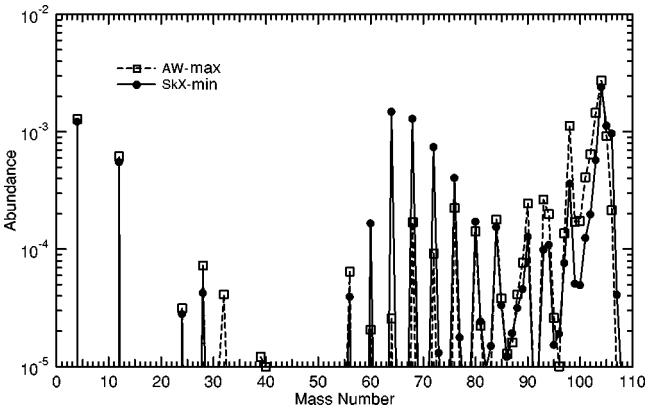


FIG. 9. Final abundance distribution summed over mass numbers for a calculation with the lowest-proton-capture $Q$ values within the uncertainties of the mass predictions of this paper (Sk$X$-min) and with the largest-proton-capture $Q$ values within the uncertainties of AW95 (AW-max).

## V. SUMMARY AND CONCLUSIONS

We have made a new set of predictions for the masses of proton-rich nuclei on the basis of the displacement energies obtained from spherical Hartree-Fock calculations with the Sk$X_{csb}$ Skyrme interaction [12,13]. Sk$X_{csb}$ provides a large improvement in the displacement energies over those obtained with other Skyrme interactions via the addition of a one-parameter charge-symmetry breaking component [13]. A comparison with the experimental displacement energies measured in the mass region $A=41$–59 indicates that the accuracy of the calculated displacement energies is about 100 keV. We thus use this as a measure of the uncertainty expected for the higher mass region of interest in this paper. Experimental masses for some proton-rich nuclei in the mass region $A=60$–70 will be required to test our predictions. At the upper end, we may expect some deviation due to the very deformed shapes that involve the excitation of many $pf$-shell nucleons into the $g_{9/2}$ $(sdg)$ shell that go beyond our spherical approach. In addition to the application to the $rp$ process, we have discussed the implication of the present model for the proton drip line. The most promising candidates for diproton emission are $^{64}$Zn, $^{59}$Ge, $^{63}$Se, $^{67}$Kr, and $^{71}$Sr.

Our $rp$ process calculations based upon the masses obtained in the present model and those obtained from the Audi-Waptra mass extrapolations demonstrate clearly the sensitivity of x-ray burst tails on nuclear masses at and beyond the $N=Z$ line between Ni and Sr. Such a sensitivity on the $Q$ values for proton capture on $^{64}$Ge and $^{68}$Se has been pointed out before by Koike *et al.* [5] based on a similar x-ray burst model. However, Koike *et al.* [5] used a limited reaction network including only nuclei up to Kr. As we show in this paper, this is not sufficient for any assumption on nuclear masses, and as a consequence we find very different light curves and final abundances.

Our new calculation leads to tighter constraints on proton-capture $Q$ values as compared with the AW95 mass extrapolations (see Fig. 7). Radioactive beam experiments including the nonobservation of $^{69}$Br and $^{73}$Rb have also begun to provide important constraints. If those experiments are taken into account, our new predictions do not lead to substantially tighter limits, with the exception of the proton capture on $^{64}$Ge, where no experimental upper limit on the proton-capture $Q$ value exists. Our new calculations increase the minimum $\beta$ branching at $^{64}$Ge by an order of magnitude from 1% to 14%, leading to a lower limit of the average $^{64}$Ge half-life in the $rp$ process of 12.6 s instead of 0.9 s. As a consequence, we predict a smooth and continuous drop in the light curve during the first 30–40 s after the maximum, as opposed to the hump predicted with AW-max.

However, uncertainties in the mass predictions are still too large to sufficiently constrain the light curves and to determine the role that proton captures play in the reduction of waiting point lifetimes. While we find that within the errors of our mass predictions proton capture on $^{72}$Kr is negligible,

TABLE II. Nuclei for which more a accurate mass would improve the accuracy of *rp* process calculations in type I x-ray bursts. The upper part of the table lists nuclei for which the current uncertainties lead to large uncertainties in calculated burst time scales. The lower part of the table lists nuclei, for which accurate masses are important, but current estimates of the uncertainties do not lead to large uncertainties in *rp* process calculations. Nevertheless, an experimental confirmation for the masses being in the estimated range would be important. Within each part, the nuclei are sorted by uncertainty, so a measurement of the top ranked nuclei would be most important. For each nucleus we list either the experimental mass excess (Expt) (Refs. [7] and [18] for $^{70}$Se) or the theoretical mass excess (Sk*X*) calculated in this work in MeV.

| Nuclide | Expt. | Sk*X* |
|---|---|---|
| $^{68}$Se | | $-54.15\pm0.30$[a] |
| $^{64}$Ge | $-54.43\pm0.250$ | |
| $^{70}$Kr | | $-40.98\pm0.16$ |
| $^{70}$Se[b] | $-61.60\pm0.12$ | |
| $^{65}$As | | $-46.70\pm0.14$ |
| $^{69}$Br | | $-46.13\pm0.11$ |
| $^{66}$Se | | $-41.85\pm0.10$ |
| $^{72}$Kr | $-54.11\pm0.271$ | |
| $^{73}$Rb | | $-46.27\pm0.17$ |
| $^{73}$Kr[b] | $-56.89\pm0.14$ | |
| $^{74}$Sr | | $-40.67\pm0.12$ |
| $^{61}$Ga | | $-47.14\pm0.10$ |
| $^{62}$Ge | | $-42.38\pm0.10$ |

[a]Theoretical estimate from AW95.

[b]Mirror to an *rp* process nucleus—a more accurate mass measurement could reduce the error in the mass prediction for the proton rich mirror nucleus by more than 30%.

our predicted average proton-capture branchings for $^{64}$Ge and $^{68}$Se still cover a large range of 0.5–86 % and 0.0–26 %, respectively (of course this is a model-dependent result—for example, more hydrogen or a higher density could strongly increase the proton-capture branches). To a large extent this is because of the large uncertainties in the masses of $N=Z$ nuclei $^{64}$Ge (measured: 270 keV), $^{68}$Se (AW95 extrapolated: 310 keV), and $^{72}$Kr (measured: 290 keV) [7] that cannot be determined with the method presented here. In addition, uncertainties in the masses of mirror nuclei increase the errors for $^{73}$Rb (170 keV) and $^{70}$Kr (160 keV) substantially beyond the $\approx$100-keV accuracy of our predicted Coulomb shifts. Overall, this results in typical uncertainties of the order of 300 keV for several of the critical proton-capture *Q* values.

To summarize, uncertainties in the masses of the nuclei that determine the proton-capture branches on $^{64}$Ge and $^{68}$Se represent a major nuclear physics uncertainty in x-ray burst light curve calculations. The relevant nuclei are listed in the upper part of Table II together with the currently available mass data and their uncertainties. The proton-capture branches on $^{60}$Zn and $^{72}$Kr are of similar importance, but are sufficiently well constrained by current experimental limits and theoretical calculations. However, both the experimental and the theoretical limits are strongly model dependent. Therefore, improved experimental mass data would still be important to confirm the present estimates. These nuclei are listed in the lower part of Table II. As discussed in Sec. III there is experimental evidence indicating proton stability of all the nuclei listed, except for $^{69}$Br and $^{73}$Rb, which are probably proton unbound [28]. Mass measurements of the proton bound nuclei could be performed with a variety of techniques including ion trap measurements, time-of-flight measurements, or $\beta$ decay studies. Recent developments in the production of radioactive beams allow many of the necessary experiments to be performed at existing radioactive beam facilities such as ANL, GANIL, GSI, ISOLDE, ISAC, and the NSCL. Mass measurements of the proton unbound nuclei $^{69}$Br and $^{73}$Rb require their population via transfer reactions from more stable nuclei, or by $\beta$ decay from more unstable nuclei. Both are significantly more challenging as much higher beam intensities or the production of more exotic nuclei are required, respectively.

Of course, burst time scales depend sensitively on the amount of hydrogen that is available at burst ignition. The more hydrogen that is available the longer the *rp* process and the longer the burst tail time scale. In this paper, we use a model with a large initial hydrogen abundance (close to solar) to explore the impact of mass uncertainties on x-ray burst light curves. This allows us to draw conclusions on the uncertainties in predictions of the longest burst time scales and the heaviest elements that can be produced in x-ray bursts. The former is important, for example, in light of recent observations of very long thermonuclear x-ray bursts from GX 17+2 [30], the latter for the question of the origin of *p* nuclei discussed below. Nevertheless we expect a similar light curve sensitivity to masses for other models as long as there is enough hydrogen for the *rp* process to reach the $A=74$–$76$ mass region. In our one-zone model we find that this requires about a 0.35–0.45 hydrogen mass fraction at ignition. Even though the burst temperatures and densities vary somewhat with the initial conditions we find shorter, but otherwise very similar reaction paths governed by the same waiting point nuclei. For bursts with initial hydrogen abundances below $\approx$0.3 the *rp* process does not reach the $A=60$–$72$ mass region anymore and the mass uncertainties discussed in this paper become irrelevant.

Observed type I x-ray bursts show a wide variety of time scales ranging from 10 s to hours. Our goal is to improve the underlying nuclear physics so that the observed burst time scales can be used to infer tight constraints on ignition conditions in type I x-ray bursts such as the amount of hydrogen available for a given burst. Such constraints would be extremely useful as they could, for example, lead to constraints on the impact of rotation and magnetic fields on the fuel distribution on the neutron star surface as well as on the heat flux from the neutron star surface [29,31]. Our results indicate that without further theoretical or experimental improvements on nuclear masses it will not be possible to obtain such tight, quantitative constraints.

Nevertheless, some qualitative conclusions can already be drawn on the basis of our new mass predictions. Our new results provide strong support for previous predictions that the *rp* process in the $A=64$–$72$ mass region slows down

considerably leading to extended burst tails [6]. As a consequence, the long bursts observed for example in GS 1826−24 [31] can be explained by the presence of large amounts of hydrogen at ignition and can therefore be interpreted as a signature of the *rp* process.

Even for our lowest-proton-capture $Q$ values, when $^{68}$Se and $^{72}$Kr slow down the *rp* process with their full $\beta$-decay lifetime the *rp* process still reaches the SnSbTe cycle. Clearly, such a slowdown of the *rp* process does not lead to a premature termination of the *rp* process as has been suggested previously (for example, Ref. [2]), but rather extends the burst time scale accordingly. As a consequence we find that hydrogen is completely consumed in our model.

However, a slower *rp* process will produce more nuclei in the $A=64-72$ range and less nuclei in the $A=98-103$ mass range. Interestingly, among the most sensitive abundances beyond $A=72$ is $^{98}$Ru, which is of special interest as it is one of the light *p* nuclei whose origin in the universe is still uncertain. *p* nuclei are proton-rich, stable nuclei that cannot be synthesized by neutron-capture processes. While standard *p* process models can account for most of the *p* nuclei observed, they cannot produce sufficient amounts of some light *p* nuclei such as $^{92,94}$Mo and $^{96,98}$Ru (for example, Ref. [32]). Costa *et al.* [33] pointed out recently that a increase in the $^{22}$Ne$(\alpha,n)$ reaction rate by a factor of 10−50 above the presently recommended rate could help solve this problem, but recent experimental data seem to rule out this possibility [34]. Alternatively, x-ray bursts have been proposed as nucleosynthesis site for these nuclei [3,6]. An accurate determination of the $^{98}$Ru production in x-ray bursts requires, therefore, accurate masses in the $A=64-72$ mass range. Further conclusions concerning x-ray bursts as a possible *p* process scenario have to wait for future self-consistent multizone calculations with the full reaction network, that include the transfer of the ashes into the interstellar medium during energetic bursts.

## ACKNOWLEDGMENT

Support for this work was provided from U.S. National Science Foundation Grants Nos. PHY-0070911 and PHY-95-28844.

[1] R. K. Wallace and S. E. Woosley, Astrophys. J. Suppl. **45**, 389 (1981).
[2] L. Van Wormer *et al.*, Astrophys. J. **432**, 326 (1994).
[3] H. Schatz *et al.*, Phys. Rep. **294**, 167 (1998).
[4] H. Schatz, L. Bildsten, A. Cumming, and M. Wiescher, Astrophys. J. **524**, 1014 (1999).
[5] O. Koike, M. Hashimoto, K. Arai, and S. Wanajo, Astron. Astrophys. **342**, 464 (1999).
[6] H. Schatz *et al.*, Phys. Rev. Lett. **86**, 3471 (2001).
[7] G. Audi and A. H. Wapstra, Nucl. Phys. **A595**, 409 (1995).
[8] B. A. Brown, Phys. Rev. C **42**, 1513 (1991).
[9] W. E. Ormand, Phys. Rev. C **53**, 214 (1996).
[10] W. E. Ormand, Phys. Rev. C **55**, 2407 (1997).
[11] B. J. Cole, Phys. Rev. C **54**, 1240 (1996).
[12] B. A. Brown, Phys. Rev. C **58**, 220 (1998).
[13] B. A. Brown, W. A. Richter, and R. Lindsay, Phys. Lett. B **483**, 49 (2000).
[14] A. Volya, B. A. Brown, and V. Zelevinsky, Phys. Lett. B **509**, 37 (2001).
[15] W. A. Richter, M. G. van der Merwe, R. E. Julies, and B. A. Brown, Nucl. Phys. **A523**, 325 (1991).
[16] M. Hjorth-Jensen, T. T. S. Kuo, and E. Osnes, Phys. Rep. **261**, 125 (1995).
[17] S. Raman, C. W. Nestor, and P. Tikkanen, At. Data Nucl. Data Tables (to be published).
[18] B. E. Tomlin *et al.*, Phys. Rev. C **63**, 034314 (2001).
[19] B. Blank *et al.*, Phys. Rev. Lett. **74**, 4611 (1995).
[20] J. Winger *et al.*, Phys. Lett. B **299**, 214 (1993).
[21] J. D. Robertson *et al.*, Phys. Rev. C **42**, 1922 (1990).
[22] R. Pfaff *et al.*, Phys. Rev. C **53**, 1753 (1996).
[23] M. F. Mohar *et al.*, Phys. Rev. Lett. **66**, 1571 (1991).
[24] A. Jokinen *et al.*, Z. Phys. A **355**, 227 (1996).
[25] Z. Janas *et al.*, Phys. Rev. Lett. **82**, 295 (1999).
[26] L. Bildsten, in *The Many Faces of Neutron Stars*, edited by A. Alpar, L. Bucceri, and J. Van Paradijs (Dordrecht, Kluwer, 1998); astro-ph/9709094.
[27] P. Möller, W. D. Myers, and J. R. Nic, At. Data Nucl. Data Tables **59**, 185 (1995).
[28] T. Rauscher and F.-K. Thielemann, At. Data Nucl. Data Tables **75**, 1 (2000).
[29] L. Bildsten, in *Rossi 2000: Astrophysics with the Rossi X-ray Timing Explorer*, Greenbelt, MD, 2000, p. E65.
[30] E. Kuulkers *et al.*, Astron. Astrophys. (submitted); astro-ph/0105386.
[31] A. Kong *et al.*, Mon. Not. R. Astron. Soc. **311**, 405 (2000).
[32] M. Rayet *et al.*, Astron. Astrophys. **298**, 517 (1995).
[33] V. Costa *et al.*, Astron. Astrophys. **358**, L67 (2000).
[34] M. Jaeger *et al.*, Phys. Rev. Lett. **87**, 202501 (2001).